Lawrence Berkeley National Laboratory
LBL Publications

Title

The seeds and homogeneous nucleation of photoinduced nonthermal melting in semiconductors due to self-amplified local dynamic instability

Permalink
https://escholarship.org/uc/item/2k20s9tq

Journal
Science Advances, 8(27)

ISSN
2375-2548

Authors
Liu, Wen-Hao
Luo, Jun-Wei
Li, Shu-Shen
et al.

Publication Date
2022-07-08

DOI
10.1126/sciadv.abn4430

Copyright Information
This work is made available under the terms of a Creative Commons Attribution License, available at https://creativecommons.org/licenses/by/4.0/

Peer reviewed

eScholarship.org Powered by the California Digital Library
University of California

PHYSICAL SCIENCES

The seeds and homogeneous nucleation of photoinduced nonthermal melting in semiconductors due to self-amplified local dynamic instability

Wen-Hao Liu[1,2], Jun-Wei Luo[1,2]*, Shu-Shen Li[1,2], Lin-Wang Wang[3]*

Copyright © 2022 The Authors, some rights reserved; exclusive licensee American Association for the Advancement of Science. No claim to original U.S. Government Works. Distributed under a Creative Commons Attribution NonCommercial License 4.0 (CC BY-NC).

Laser-induced nonthermal melting in semiconductors has been studied over the past four decades, but the underlying mechanism is still under debate. Here, by using an advanced real-time time-dependent density functional theory simulation, we reveal that the photoexcitation-induced ultrafast nonthermal melting in silicon occurs via homogeneous nucleation with random seeds originating from a self-amplified local dynamic instability. Because of this local dynamic instability, any initial small random thermal displacements of atoms can be amplified by a charge transfer of photoexcited carriers, which, in turn, creates a local self-trapping center for the excited carriers and yields the random nucleation seeds. Because a sufficient amount of photoexcited hot carriers must be cooled down to band edges before participating in the self-amplification of local lattice distortions, the time needed for hot carrier cooling is the response for the longer melting time scales at shorter laser wavelengths. This finding provides fresh insights into photoinduced ultrafast nonthermal melting.

INTRODUCTION

Ultrashort laser pulses are now used to manipulate the structure and function of materials at far from equilibrium states (*1*–*9*), with the corresponding ultrafast dynamics being one of the ultimate problems in modern science and technology. In terms of applications, the femtosecond and nanosecond pulsed laser was first used to deal with the annealing of the amorphous layer of ion-implanted silicon (Si) in the late 1970s (*10*) and then extended to annealing the lattices of other semiconductors, such as Si (*11*–*23*), GaAs (*2*, *15*, *24*, *25*), InSb (*1*, *3*, *26*–*29*), and Ge (*30*, *31*). Soon after the discovery of the so-called pulsed laser annealing, it was established that this laser annealing is an ultrafast nonthermal melting process (*32*–*35*) in which the photoexcited electrons are hot and the ions are still cold (in terms of kinetic energy) because the lattice disordering starts and finishes well before the completion of carrier-lattice thermalization via electron-phonon coupling. Specifically, at sufficiently high levels of photoexcitation, the loss of long-range order inside semiconductor lattices was observed to exist on a subpicosecond time scale (*1*), arising from a strong modification of the interatomic potential owing to the photoexcitation of a substantial amount (10% or more) of electrons from the valence band to the conduction band. This is in sharp contrast to the laser-induced thermal melting in metals, which exists on a time scale of tens of picoseconds due to the required time for electron-lattice equilibration to heat the lattice above the melting point (*36*, *37*), followed by liquid nucleation on the surface and spreading out with a liquid front propagating at most at the speed of sound (1.5×10^3m/s for Si) (*37*–*39*).

Pulsed laser annealing in semiconductors has also generated intensive debate over the past four decades about its underlying microscopic mechanisms. It is commonly believed that, on the subpicosecond time scale, the excitation of a large fraction of electrons from bonding valence bands to antibonding conduction bands could weaken the lattice and induce a repulsive interatomic force to quickly disorder the lattice without remarkably increasing its thermal energy (*1*–*3*). The debate now focuses on the mechanisms and microscopic picture for such a disorder occurs, whether driven by softened phonon modes with an imaginary frequency [corresponding to a saddle point on the potential energy surface (PES)] (*14*, *15*, *20*, *28*) or by the random velocity of each atom while there is a flat PES (*3*, *29*, *40*). The former is termed electron-hole plasma-induced phonon instability theory (*11*), and the latter is the so-called inertial model (*3*). Stampfli and Bennemann (*41*) used a tight-binding theory to simulate the laser pulse–induced melting of Si, Ge, and diamond, claiming to derive a dense electron-hole plasma by populating the single-particle energy levels according to the Fermi-Dirac distribution with an artificially high electron temperature. This plasma represents the laser pulse excitation of valence electrons, although it usually takes approximately 1 ps for the carrier distribution to reach equilibrium from a Fermi-Dirac distribution (*2*). The dense electron-hole plasma is found to soften and stabilize the transverse acoustic phonons (*14*) and/or the longitudinal optical phonons (with an imaginary frequency) (*15*, *28*), which then drives distortion of the lattice. This is a two-temperature model, assuming that the electron and lattice have two different temperatures, but each system is in equilibrium. The direct probe of the atomic structure change using the ultrafast time-resolved x-ray diffraction and the observation of little variation as the laser fluence changes from 50 to 100 mJ/cm^2 led Lindenberg *et al.* (*3*) to formulate an alternative inertial model. The idea behind the inertial model is that the unbound atoms move at the random velocity they had at the time when the bonds were broken. This model is further supported by the finding of temperature-dependent melting rates because the initial random velocities are set by the thermodynamic temperature (*29*). However, this has also been disputed by Zijlstra *et al.* (*28*) based on an ab initio density functional theory (DFT) prediction that dense electron-hole plasma softens only the acoustic phonon rather than all modes, as assumed in the inertial model. Hartley *et al.* (*42*) showed that melting is faster than that predicted by the inertial model. The observation of forces

[1]State Key Laboratory of Superlattices and Microstructures, Institute of Semiconductors, Chinese Academy of Sciences, Beijing 100083, China. [2]Center of Materials Science and Optoelectronics Engineering, University of Chinese Academy of Sciences, Beijing 100049, China. [3]Materials Science Division, Lawrence Berkeley National Laboratory, Berkeley, CA 94720, USA.
*Corresponding author. Email: jwluo@semi.ac.cn (J.-W.L.); lwwang@semi.ac.cn (L.-W.W.)

acting on the atoms after bond breaking led to an additional Coulomb force model (*42*, *43*), where the photoexcitation of a large fraction of valence electrons was suggested to trigger the Coulombic repulsion between ions to immediately disorder the lattice.

However, all these models are difficult to understand because the melting effect varies depending on the laser wavelength. Evidence has accumulated that a shorter melting time scale in Si is due to a longer laser wavelength: Laser pulses of 2.03 eV give rise to nonthermal melting within 100 to 200 fs (*12*), but a shorter laser wavelength of 3.2 eV offers slower melting, with a time scale of approximately 500 fs (*13*). Longer melting time is considered to be the result of a delayed onset of the nonthermal melting event, which is currently interpreted as the time needed for the secondary electron cascade to thermalize the electronic system (*21*). Furthermore, all these models suggest that nonthermal melting should develop uniformly at atomic scale for the area under irradiation (*29*, *40*). However, this cannot be resolved experimentally, as the probing techniques of ultrafast electron (*4*, *5*, *37*) and x-ray (*1*, *3*) diffraction and ultrafast optical spectroscopy (*44*, *45*) all measure averaged results over many unit cells, and, thus, they are less sensitive to an atomic-scale microscopic melting pattern.

Here, we reveal that photoinduced ultrafast nonthermal melting occurs via homogeneous nucleation with randomly distributed local seeds rather than simultaneously breaking all the bonds, as suggested by proposed mechanisms. We use newly developed real-time time-dependent DFT (rt-TDDFT) by introducing a Boltzmann factor to restore the detailed balance, which is capable of describing the hot carrier cooling process (*46*, *47*) to perform first-principles simulations of the photoexcitation-induced nonthermal melting in Si. Without "ad hoc" hypotheses, our simulations closely reproduce experimental data using both 387-nm (3.2 eV) and 610-nm (2.03 eV) laser pulses. This unprecedented agreement affirms the reliability of our method and allows us to study the microscopic mechanism behind the laser wavelength–dependent melting process. We further reveal that the nonthermal melting is initiated at atomic sites by lattice vibrations induced by random atomic displacements (nucleation of the liquid phase) and is amplified by the spatial localization of photoexcited carriers populated at the band-edge states. This localization leads to the dynamic instability of the local lattice and creates a self-trapping center for other carriers, which leads to a positive feedback amplification and causes local melting nucleation. These atomic-scale nucleation seeds are initially distributed randomly over the laser-irradiated layer. They are followed by rapid growth in size and finally connecting, yielding a complete system nonthermal melting within 200 fs. A sufficient amount of photoexcited hot carriers must be cooled down to the band edges before participating in the amplification of local lattice distortions via self-trapping. The time needed for the cooling of this hot carrier (rather than electron-lattice equilibration) is the response for the longer melting time scales at shorter laser wavelengths, as observed experimentally for Si (*13*).

RESULTS

Laser wavelength–dependent melting

To reveal the physics underlying laser wavelength–dependent melting, we investigated the atomic dynamics of the ultrashort laser pulse–induced melting of Si using two different laser wavelengths following experiments (*12*, *13*). This investigation was carried out by performing rt-TDDFT simulations for photoexcited Si at an initial temperature of 300 K. Following the rt-TDDFT simulations, to directly compare the experimental data, we also computed the x-ray diffraction intensity $I(t)$ based on the Debye-Waller formula (*3*, *13*, *20*), $I(t) = \exp[-Q^2\langle u^2(t)\rangle/3]$, where Q is the reciprocal lattice vector corresponding to the x-ray reflection peak and $u^2(t)$ is the square of the root mean square displacement (RMSD) averaged over all atoms. Figure 1A shows that the simulated $I(t)$ is in excellent agreement with the experimental data for photoexcitation at both laser wavelengths, showing that the laser wavelength has a substantial influence on the melting process. The quantitative agreement with the experiment affirms the accuracy and reliability of our simulations. We reveal a nonintuitive phenomenon that the lower-energy photons cause a much faster nonthermal melting than the high-energy photons (Fig. 1A), although the 387-nm laser pulse deposits 1.6 times more energy in the system than the 610-nm laser pulses, both exciting the same amount (11%) of valence electrons into the conduction bands.

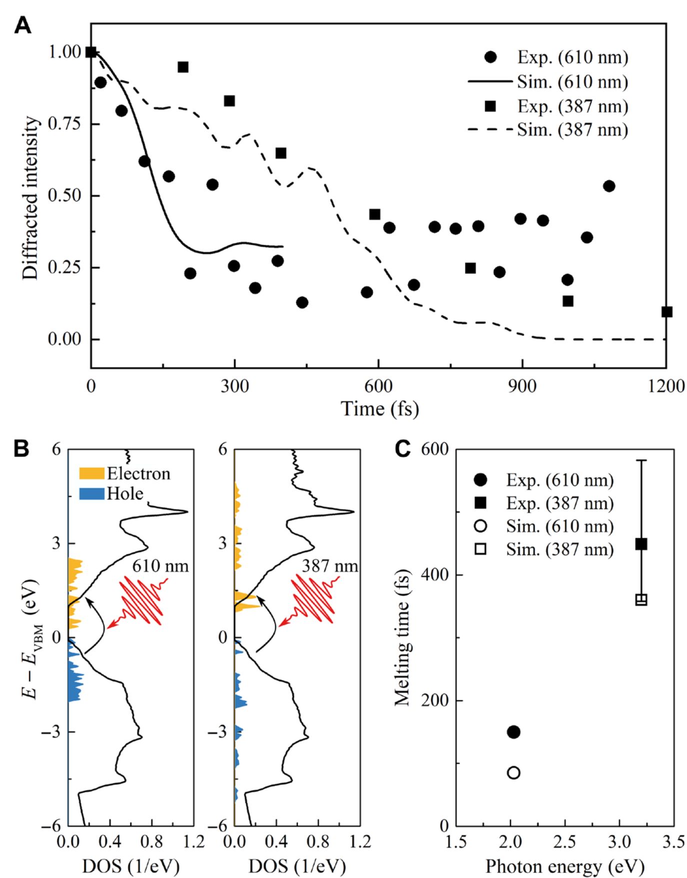

Fig. 1. Simulation of laser-induced ultrafast nonthermal melting of Si irradiated by two laser pulses with 610- and 387-nm wavelengths. (**A**) The rt-TDDFT simulations predicted the dynamic evolution of diffracted intensity following the photoexcitation of 11% of valence electrons by 610-nm (solid line) and 387-nm (dashed line) laser wavelength, respectively, in comparison with experimental data [filled circles for 610-nm laser (*12*) and filled square for 387-nm laser (*13*)]. (**B**) Population of energy levels of photoexcited electrons (yellow area) and holes (blue area) at 100 fs following photoexcitation. The black solid line represents the density of states (DOS) of unperturbed bulk Si, where the valence band maximum (VBM) is set to 0 eV and the conduction band minimum (CBM) is at 1.12 eV. (**C**) Predicted Si melting (or disordering) times depending on the photon energy (or laser wavelength) is compared with experimental data from Tom *et al.* (*12*) (610-nm wavelength) and Harb *et al.* (*13*) (387-nm wavelength).

The predicted nonthermal melting times agree with experiments within the experimental error bars and demonstrate that the melting rate (1/time) is inversely proportional to the photon energy, as shown in Fig. 1C. Notably, we have used the onset of the experimental diffraction pattern change as the unifying reference time ($t = 0$) to calculate their melting time. The different melting processes can be traced back to the distinct distribution of photoexcited electrons and holes within the conduction and valence bands, as shown in Fig. 1B. We can see that the 610-nm laser pulse excites the valence electrons mostly from the top part of the valence band to populate the bottom part of the conduction band, whereas the 387-nm laser pulse promotes the electrons from the deeper part of the valence band into the higher energy levels in the conduction band, spanning a wide energy range of the valence and conduction bands. We also note that a fast nonthermal melting within 100 fs has been reported by the x-ray pump (*42*), which, at first glance, is against our finding because the x-ray pump should prompt valence electrons from deeper levels in the valence bands to much higher energy levels in the conduction bands. In figs. S4 and S5, our rt-TDDFT simulations illustrate that if 11% valence electrons were prompted to higher energy states up to 20 eV above the conduction band minimum, then nonthermal melting is unlikely to occur within a short time scale. Note that we do not consider other effects (such as photoemission and Auger decay) in such higher energy excitation. In reality, in x-ray pumping, the decay of the extremely hot carriers to the band edges is much faster via the Auger process, which cannot be described in our TDDFT simulation. Furthermore, this double excitation can also increase the concentration of excited carriers. These two factors can both remarkably reduce the melting time. As a result, our conclusion is not in contradiction with the x-day pumping experiment. However, we still have to stress that if the laser energy is not so high (as to cause the second excitation through Auger), then, for the same fluence, the higher frequency might cause a slower melting due to the need for hot carrier relaxation to the band edges through electron-phonon coupling.

DISCUSSION

The emergence of nucleation seeds

We now examine the detailed atomic dynamics of Si following irradiation with a 610-nm laser pulse exciting 11% of valence electrons according to experiments (*12*). Following common practice in the literature (*18*), we adopt RMSD to characterize the degree of the loss of long-range atomic disorder (or melting). The usual criterion used to determine melting is the Lindemann criterion at 15% (*18*, *20*), which is RMSD = 0.35 Å, as the Si equilibrium bond length is 2.35 Å, as indicated by the dashed line in Fig. 2C. We find that the value of RMSD increases monotonically during the first 200 fs following photoexcitation: It reaches the Lindemann criterion (0.35 Å) at approximately 100 fs and continues to grow to 0.8 Å at 200 fs, as shown in Fig. 2A. It is interesting to see in Fig. 2B that, throughout the whole simulation, the lattice remains relatively cool with a temperature of approximately 450 K, which is far below the melting temperature of Si (1680 K) (*16*). This demonstrates a nonthermal melting process.

To reveal the microscopic details of the nonthermal melting, we plot a series of snapshots with time (0, 50, 80, and 100 fs following photoexcitation) for atomic structures of photoexcited Si in Fig. 2E. We render atoms with displacements exceeding 0.35 Å (so-called "Lindemann particles") in red in Fig. 2E. These Lindemann particles consisting of single atoms emerge as early as 50 fs (Fig. 2D), although melting deduced from the diffraction intensity starts only at 100 fs and completes (indicated by the minimum in the diffraction intensity) at 200 fs. Afterward, these Lindemann particles develop into a cluster, which grows rapidly in size, as illustrated in the 80- and 150-fs snapshots. Consequently, the molten atoms in each supercell spread outward and then connect with its nearest-neighbor images in the supercell calculation, yielding ultrafast nonthermal melting throughout the whole system within 200 fs. In short, these Lindemann particles occur randomly and statistically inside the bulk crystal and are interpreted as the seeds for melting nucleation, which eventually causes melting of the whole system, as schematically illustrated in Fig. 2F. In addition, we also calculate the pair distribution function to further illustrate the local nonthermal melting in Si (fig. S3).

We thus reveal that nonthermal melting occurs via a homogenous nucleation process with randomly distributed local seeds, rather than all at once throughout the Si crystal in an atomic-scale uniform fashion, as suggested by the inertial model (*3*) and phonon instability theory (due to the simultaneous breaking of all bonds caused by the excitation of high-density electron-hole plasma) (*14*, *15*). It has been established that homogeneous nucleation is a mechanism for the rapid thermal melting of superheated metals within several picoseconds (*36*, *37*, *39*, *48*, *49*). It was predicted that, in superheated metals, the vibrational and mechanical instabilities of the lattice occur simultaneously but only locally, leading to the formation of destabilized clusters inside the bulk (*50*). The melting rate is mostly governed by electron-lattice equilibration (approximately several picoseconds) to heat the atoms in the metal to a superheated state. In our semiconductor case, electron-lattice equilibrium is not realized at the nonthermal melting time, and our melting is not caused by superheating. While the nucleation phenomenon appears to be the same, the atomistic mechanisms causing these local nucleations are different.

The microscopic mechanism underlying the birth of nucleation seeds

We delineate the factors that break the spatial translational symmetry and locally cause atomic disorders as seeds of homogeneous nucleation. The Lindemann particles emerge as early as 50 fs, which is in the middle of the laser pulse irradiation because the laser pulse duration is approximately 100 fs. This means the melting starts even when the laser has only excited 9% of valence electrons, which is less than the threshold predicted under the electron-hole plasma model (*14*, *15*, *41*). In our above simulations, the system is in equilibrium at room temperature before the photoexcitation. There are all kinds of phonons in Si, such as the acoustic and optical phonons at the zone center belonging to symmetry-breaking T_{1u} and T_{2g} group representations, respectively, rather than the A_{1g} representation that is the only phonon mode for the lattice to vibrate while preserving symmetry. The thermal random movements of atoms of the phonon modes and the associated breaking of translational symmetry can obscure the analysis of electronic properties and interatomic forces, hindering the disclosure of origin of the birth of nucleation seeds. For instance, the real-space distribution of photoexcited electrons for a snapshot at 20 fs exhibits nonuniformity, as shown in Fig. 2E. This randomness can obscure the true reason for the nucleation. To suppress the effects of these thermal random movements, we repeated the simulation for a 610-nm laser pulse at a low initial temperature

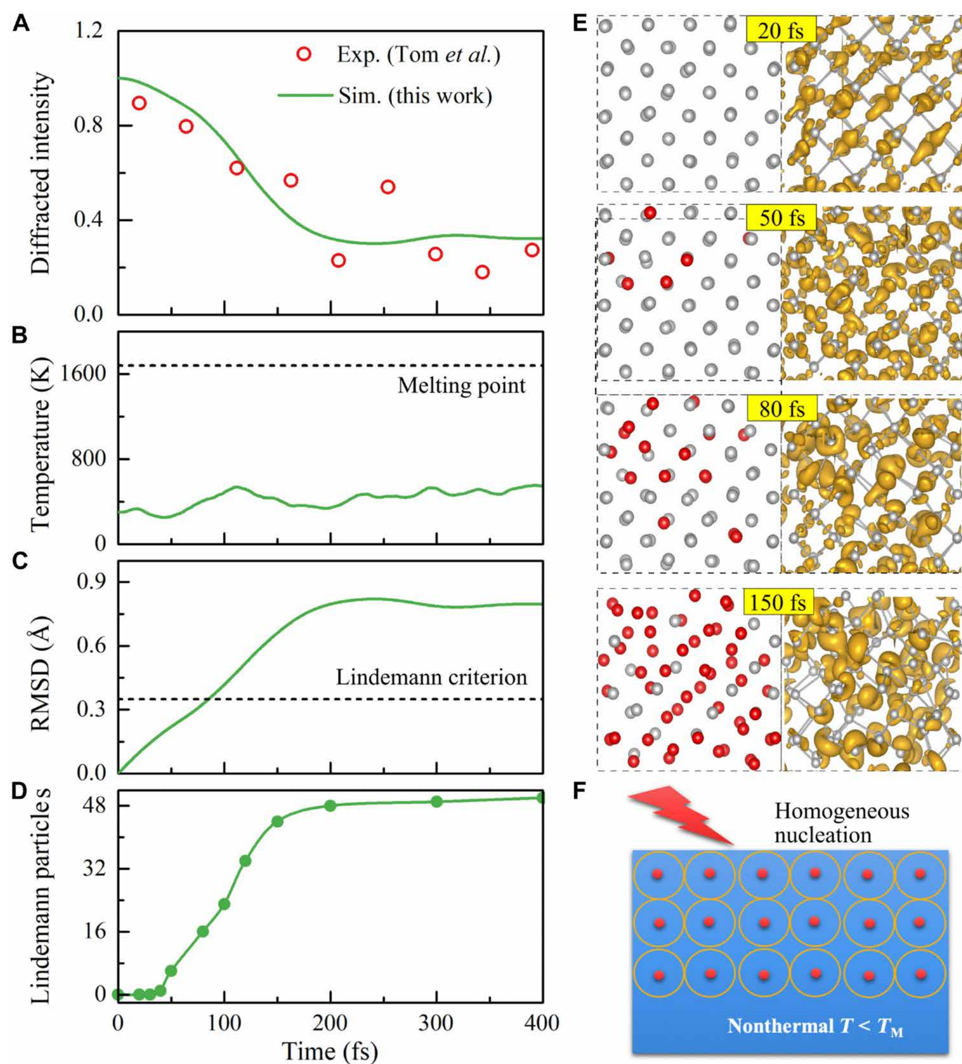

Fig. 2. Atomic dynamics of laser-induced ultrafast melting of Si irradiated with a 610-nm, 100-fs laser pulse. (**A**) Time-dependent diffraction intensity obtained directly from the evolution of atomic positions in the rt-TDDFT simulation (green line) in comparison with the experimental data (red circles) (*12*). (**B**) Lattice temperature as a function of time following the photoexcitation. The dashed line marks the Si melting temperature $T_M = 1680$ K. (**C**) Simulation-predicted RMSD of atoms as a function of time following the photoexcitation. The dashed line indicates the Lindemann criterion, which is $R_c = 0.35$ Å for 15% of equilibrium Si—Si bond length (2.35 Å) (*18*). (**D**) Number of Lindemann particles following the photoexcitation. (**E**) Snapshots of atomic displacements (viewed along the [001] direction) with time at 0, 50, 80, and 150 fs following the photoexcitation. The red atoms indicate the Lindemann particles with displacements $R_i(t) - R_i(0) > 0.35$ Å, which represents the molten atoms. The corresponding real-space distributions of photoexcited electrons (yellow iso-surface) are at the right. (**F**) Schematically illustrated the homogeneous nucleation of the laser-induced ultrafast nonthermal melting. The red points represent the randomly distributed nucleation seeds corresponding to clusters of Lindemann particles.

of 1 K (fig. S7). At the initial stage following the photoexcitation, the photoexcited electrons and holes shown in Fig. 3A are uniformly and coherently distributed over the whole lattice. The photoexcitation induces the depletion of the bonding states and population of the antibonding states, which are not disturbed by any notable randomness at the initial time. Hence, the interatomic forces induced by the photoexcitation are uniform for all the atoms, resulting in a zero net force on each Si atom (schematically shown in Fig. 3A). However, with time, carrier localizations occur unexpectedly in both excited electrons and holes, as shown in Fig. 3C. This random localization is initiated by the thermal induced random atomic vibrations at 1 K. This localization traps the excited carriers in some local regions with lower energy, which generates non-uniform interatomic forces to cause local atomic displacement, which, in turn, traps more carriers, thus forming a positive instability loop. This leads to the formation of melting seeds. It is worth mentioning that this carrier localization, which is critical to our model, does not play any role in the inertial model, phonon softening model, and Coulomb force models. We analyze below why this local carrier trapping is dynamically unstable with a self-trapping and self-amplification effect.

One can simplify the electronic structure of bulk Si as the bonding and antibonding states of Si covalent bonds, as shown in Fig. 3 (A to C). At the ground state, the bonding states are fully occupied by valence electrons, leaving the antibonding states empty with a 1.12-eV bandgap between them. Under laser irradiation, incident photons excite electrons from the bonding states (valence band) to the

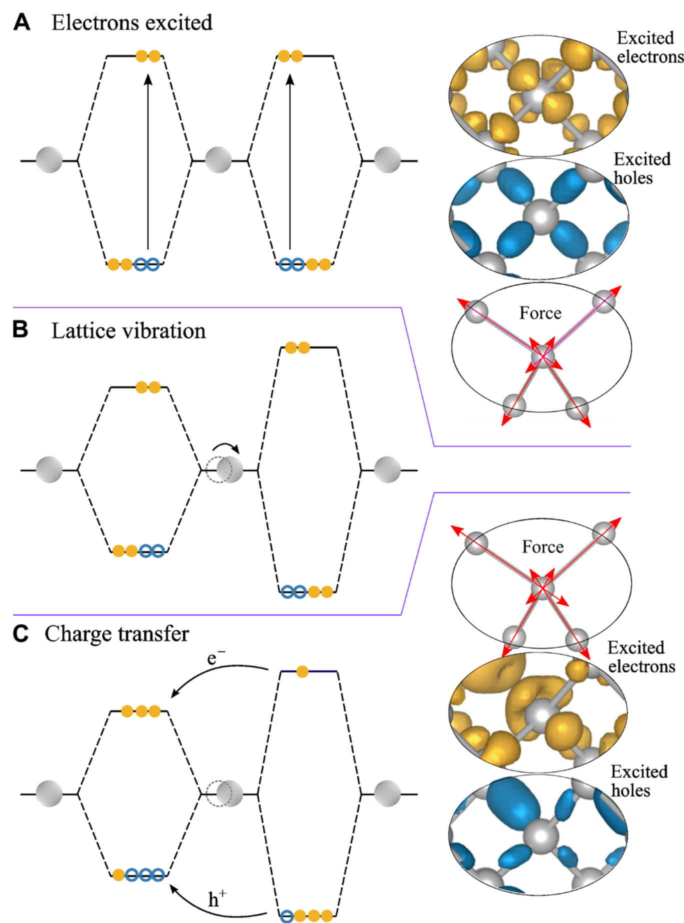

Fig. 3. Emergence of the self-trapping center due to electron-lattice coupling–induced self-amplification. (**A**) The incident photons promote valence electrons from the filled bonding states in the valence band to the empty antibonding states in the conduction band. The photoexcited electrons and holes are uniformly distributed among atom bonds, generating interatomic forces with an equivalent magnitude. (**B**) The lattice vibration–induced random movements of atoms cause local distortions in the lattice, which, in turn, yields band-edge fluctuations. (**C**) The tensile distorted region acts as a trapping center for excited electrons and holes and induces carrier localization. The carrier localization, in turn, amplifies the initial thermal random distortion. Subsequently, this process is an unstable self-trapping process and is slightly similar to the polaron to break the translational symmetry (*59*). Insets in (A) and (C) represent the real-space distribution of excited electrons and holes, as well as charge population, which generated interatomic forces immediately after photoexcitation and at 200 fs, respectively.

antibonding states (conduction band), leaving behind voids (holes) in the bonding states (Fig. 3A). The electron (hole) population of the antibonding (bonding) states raise the free energy of the excited system, which can lower its energy by lowering (raising) the energy level of the antibonding (bonding) states by elongating the Si─Si bond length. As a result, the charge population generates a stretching force on each bond. However, if everything is uniform and coherent atomically, then the starching forces at all the bonds exert a zero net force on each atom. However, if there are small fluctuations (as provided by the 1 K of thermal induced atomic vibrations), then the bond with a slightly longer length lowers (raises) the antibonding (bonding) state more than its neighbors. It further traps more electrons (holes) at the antibonding (bonding) state, causing a larger stretching force on the end atoms. This causes an imbalance in the net force at each atom, thus further stretching the bond length. This causes an unstable amplification mechanism. That is exactly what is shown in Fig. 3C. We thus propose an excited carrier localization instability with a carrier self-trapping picture. This picture is different from both the inertial model and phonon softening model. Because of the carrier localization, the density of excited electrons and holes in the local region easily exceeds the required density for phonon softening, although the corresponding overall charge density is still lower than the requirement in the phonon softening theory (*14*, *15*, *41*). This explains why the system at 50 fs with only 9% overall valence electron excitation already has some local melting at the nucleation sites.

Role of hot carrier cooling

The reason why the melting is slower when a higher-frequency laser is used remains to be explained. The increased melting time of shorter laser wavelengths has caused controversy in some studies (*12*, *13*, *22*). As we discussed above, ultrafast nonthermal melting mainly occurs because of the self-trapping of excited electrons and holes at the band-edge states, which weakens the Si─Si bonds at atomic sites. Hot carriers populated at higher energy levels have to relax to the band-edge states first before participating in the self-trapping process. Figure 1C shows that the 610-nm laser pulse excited electrons and holes are much closer to the band edges than the 387-nm laser pulse case. Higher energy states have more delocalization and, thus, have weak bonding and antibonding characteristics than the band-edge states, thus contributing less to Si─Si bond weakening. To demonstrate this further, we used a constrained DFT to calculate the PESs along the Si─Si bond stretching using carrier population, which is the same as in the cases of 610- and 387-nm laser wavelengths (fig. S8). This shows that the carrier population according to the case of a 610-nm laser wavelength can modify the PES to weaken the lattice, whereas the carrier population in the case of a 387-nm laser wavelength hardly has any effects in modifying the PES. This illustrates that ultrafast nonthermal melting is not enhanced by deposing more energy into the electronic subsystem by increasing the single-photon energy; rather, the occupations of the special states (band-edge states) are more responsible. Furthermore, we also carried out conventional rt-TDDFT simulations without the use of the Boltzmann factor technique, which cannot describe the carrier cooling process because of the lack of a detailed balance (*51*). In these conventional rt-TDDFT simulations, 387-nm laser-excited electrons and holes always occupy higher energy levels. No melting occurs during the 2-ps simulation time, and the excited carrier charge density distributes evenly in space throughout the whole Si crystal during all simulation times (Fig. 4E).

Experimental measurements have shown that under 387-nm laser pulse irradiation, nonthermal melting does occur, albeit at a longer time scale of 500 fs. In reality, excited hot carriers relax to lower energy levels through the emission of phonons and transfer excess energy into the lattice (hot carrier cooling) (*2*, *52*). Our newly developed rt-TDDFT algorithm with the Boltzmann factor (fig. S9) can describe this hot carrier cooling properly. In the Boltzmann-TDDFT simulation, our results have shown a longer time scale (~500 fs) of nonthermal melting for the 387-nm laser pulse, in excellent agreement with experimental observations (*13*), as shown in Figs. 1A and 4D. Note that the first Lindemann particle appears as early as 80 fs, implying that it originates from the localization of a small number of photoexcited carriers inside the locally distorted atomic sites due

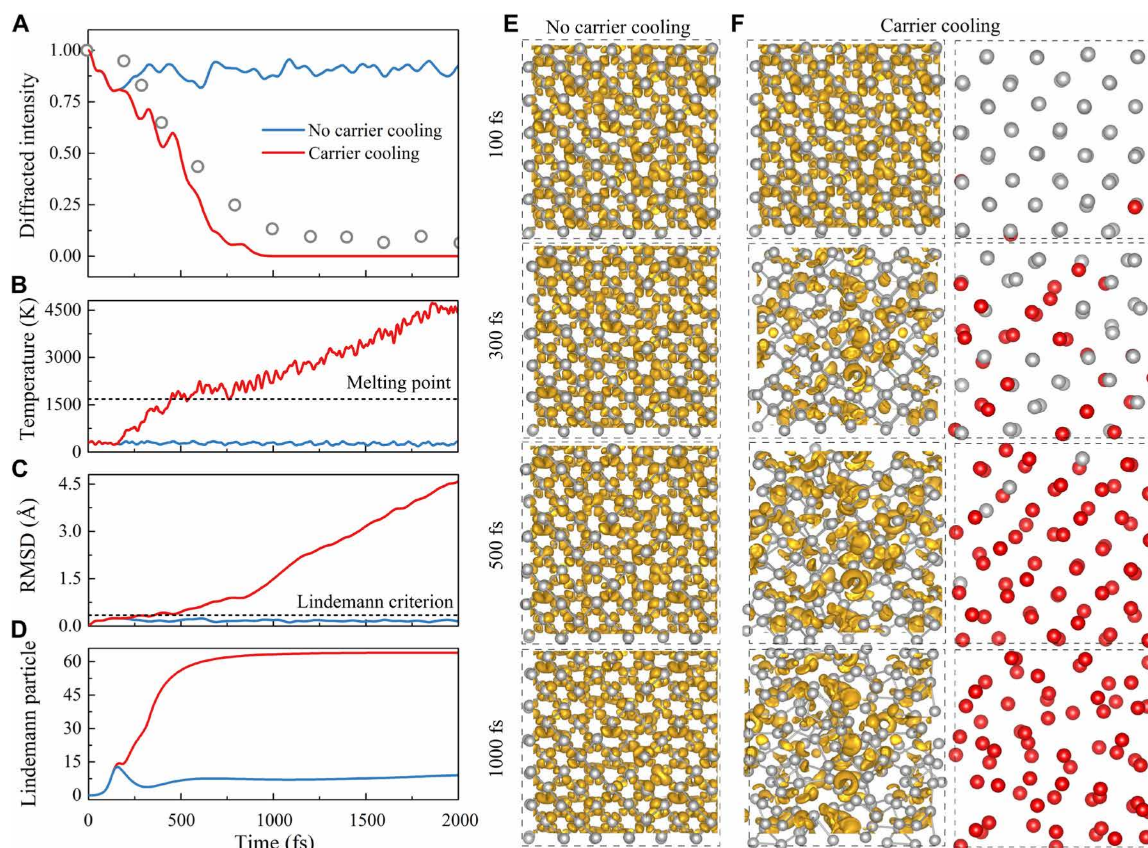

Fig. 4. Atomic dynamics of laser-induced ultrafast melting of Si irradiated with a 387-nm, 150-fs laser pulse. (**A**) The rt-TDDFT simulation predicted the electron-diffracted intensity of Si (220) Bragg peaks following the photoexcitation by a 387-nm, 150-fs pump pulse in comparison with experimental data (*13*). Here, we carry out two rt-TDDFT simulations: One takes into account the hot carrier cooling (red lines), and another has no carrier cooling, as in conventional rt-TDDFT simulations (blue lines). (**B**) Evolution of crystal temperature following the photoexcitation. (**C**) Evolution of atomic RMSD following the photoexcitation. (**D**) Evolution of the number of Lindemann particles. (**E** and **F**) Snapshoots of real-space distributions of excited electrons (yellow iso-surface) and atomic displacements with times at 100, 300, 500, and 1000 fs following the photoexcitation (E) without and (F) with taking into account carrier cooling, respectively. The red atoms indicate the Lindemann particles with displacements $R_i(t) - R_i(0) > 0.35$ Å.

to the self-trapping and self-amplification process, as we discussed above. Time is needed for more hot carriers to relax to band-edge states to participate in the growth of the nucleation seeds. This is confirmed by the fact that the lattice is heated above the melting temperature within 500 fs, as shown in Fig. 4B. Therefore, we conclude that the longer melting start time in the 387-nm laser case is due to hot carrier cooling. Overall, we show that hot carrier cooling is essential. Not only is it needed to describe the self-trapping and amplification process near the band-edge states, but also it is needed to describe the cooling from the higher energy excitation to the band-edge states.

According to our understanding, the carrier trapping by "Lindemann" particles via electron-lattice coupling is crucial for ultrafast nonthermal melting. In semiconductors, deep-level defects acting as carrier killers will certainly affect the nonthermal melting by trapping carriers. These unwanted deep-level defects have to be kept in a very low concentration for the semiconductor to be useful. Because the concentration of the photoexcited carriers is usually several orders of magnitude higher than defect concentration, we have neglected the carrier trapping caused by the defects in this study. In the future, it will be interesting to study what is the defect concentration for the defect caused by carrier trapping that becomes important.

In summary, on the basis of rt-TDDFT simulations using a newly developed Boltzmann method, we have proposed homogeneous nucleation with randomly distributed seeds arising from local instability caused by carrier self-trapping and amplifications as the microscopic mechanism for the laser-induced ultrafast nonthermal melting of semiconductors. Homogeneous nucleation has also been proposed before as a mechanism for the rapid melting of superheated metals (*37*, *48*, *50*) with a time scale above several picoseconds. In these metallic cases, the local instability is caused by the thermal vibration of the lattice. In contrast, for semiconductors, the local instability is driven mostly by the photoexcited carriers via a self-trapping and self-amplification process. This is only possible when there is a bandgap in the material (semiconductor) with bonding and antibonding states at the band edges, which is fundamentally different from the metallic case. Because of this local dynamic instability, any initial small random displacements induced by phonon vibrations can be amplified and followed by charge transfer of the photoexcited carriers, which, in turn, weakens the local bond and attracts more carriers. This amplifies the initial thermal randomness, yielding local nucleation seeds for nonthermal melting. Because a sufficient amount of photoexcited hot carriers must be cooled down to the band edges before participating in the self-amplification of

local lattice distortions, the time needed to cool this portion of hot carriers (rather than electron-lattice equilibration) is the response for the longer melting time scales at shorter laser wavelengths. Further experiments are called to verify our findings. This diffuse scattering provides a powerful tool for exploring laser-induced nonthermal melting in semiconductors in the future (*53*, *54*). For instance, total scattering of a diffuse scattering has been used to probe the atomic disordering during photoinduced phase transition in VO_2 (*54*). We believe that our results offer a comprehensive and detailed picture for nonthermal melting in semiconductors and provide fresh insights into photoinduced dynamics.

MATERIALS AND METHODS

We carry out the rt-TDDFT simulations (*55*) on the basis of norm-conserving pseudo-potentials (*56*) and the Perdew-Burke-Ernzerhof functional within a DFT framework with a plane wave nonlocal pseudo-potential Hamiltonian, which is implemented in the code PWmat (*57*). We have corrected the DFT bandgap to the Si experimental bandgap of 1.12 eV using a reasonable way, as developed in our previous work (*58*) and detailed in figs. S1 and S2. The wave functions are expanded on a plane wave basis with an energy cutoff of 50 rydberg. In rt-TDDFT simulations, we use a 64-atom supercell for Si, and the Γ point is used to sample the Brillouin zone. Our conclusions are independent on a supercell size by a comparison to the rt-TDDFT simulations with a 216-atom supercell (figs. S10 and S11). The time step is set to 0.1 fs in our dynamic simulations. The laser pulse has a wavelength $\lambda = 610$ nm, duration $\sqrt{2}\sigma = 25$ fs, and photon energy $\omega = 2.03$ eV, which is consistent with the parameters from another experiment (*12*). Another laser pulse has a wavelength $\lambda = 387$ nm, duration $\sqrt{2}\sigma = 25$ fs, and photon energy $\omega = 3.2$ eV, which is consistent with the parameters from another experiment (section S1) (*13*). The new Boltzmann factor algorithm for the rt-TDDFT can be found in (*46*) and (*47*) as well as section S3. In our simulations, we mainly use the *NVE* ensemble, in which the atomic number *N*, volume *V*, and total energy *E* are conserved. In the *NVE* ensemble, the hot carriers transfer extra energy to cold lattice through electron-phonon (el-ph) coupling, which increases the system temperature. In the *NVT* ensemble with the fixed atomic number *N*, volume *V*, and system temperature *T*, we can remove this hot carrier cooling to cause the increase of the lattice temperature.

SUPPLEMENTARY MATERIALS

Supplementary material for this article is available at https://science.org/doi/10.1126/sciadv.abn4430

REFERENCES AND NOTES

1. A. Rousse, C. Rischel, S. Fourmaux, I. Uschmann, S. Sebban, G. Grillon, P. Balcou, E. Förster, J. P. Geindre, P. Audebert, J. C. Gauthier, D. Hulin, Non-thermal melting in semiconductors measured at femtosecond resolution. *Nature* **410**, 65–68 (2001).
2. S. K. Sundaram, E. Mazur, Inducing and probing non-thermal transitions in semiconductors using femtosecond laser pulses. *Nat. Mater.* **1**, 217–224 (2002).
3. A. M. Lindenberg, J. Larsson, K. Sokolowski-Tinten, K. J. Gaffney, C. Blome, O. Synnergren, J. Sheppard, C. Caleman, A. G. MacPhee, D. Weinstein, D. P. Lowney, T. K. Allison, T. Matthews, R. W. Falcone, A. L. Cavalieri, D. M. Fritz, S. H. Lee, P. H. Bucksbaum, D. A. Reis, J. Rudati, P. H. Fuoss, C. C. Kao, D. P. Siddons, R. Pahl, J. Als-Nielsen, S. Duesterer, R. Ischebeck, H. Schlarb, H. Schulte-Schrepping, T. Tschentscher, J. Schneider, D. von der Linde, O. Hignette, F. Sette, H. N. Chapman, R. W. Lee, T. N. Hansen, S. Techert, J. S. Wark, M. Bergh, G. Huldt, D. van der Spoel, N. Timneanu, J. Hajdu, R. A. Akre, E. Bong, P. Krejcik, J. Arthur, S. Brennan, K. Luening, J. B. Hastings, Atomic-scale visualization of inertial dynamics. *Science* **308**, 392–395 (2005).
4. M. Eichberger, H. Schäfer, M. Krumova, M. Beyer, J. Demsar, H. Berger, G. Moriena, G. Sciaini, R. J. D. Miller, Snapshots of cooperative atomic motions in the optical suppression of charge density waves. *Nature* **468**, 799–802 (2010).
5. G. Sciaini, R. J. D. Miller, Femtosecond electron diffraction: Heralding the era of atomically resolved dynamics. *Rep. Prog. Phys.* **74**, 096101 (2011).
6. T. Frigge, B. Hafke, T. Witte, B. Krenzer, C. Streubühr, A. Samad Syed, V. Mikšić Trontl, I. Avigo, P. Zhou, M. Ligges, D. von der Linde, U. Bovensiepen, M. Horn-von Hoegen, S. Wippermann, A. Lücke, S. Sanna, U. Gerstmann, W. G. Schmidt, Optically excited structural transition in atomic wires on surfaces at the quantum limit. *Nature* **544**, 207–211 (2017).
7. E. A. Seddon, J. A. Clarke, D. J. Dunning, C. Masciovecchio, C. J. Milne, F. Parmigiani, D. Rugg, J. C. H. Spence, N. R. Thompson, K. Ueda, S. M. Vinko, J. S. Wark, W. Wurth, Short-wavelength free-electron laser sources and science: A review. *Rep. Prog. Phys.* **80**, 115901 (2017).
8. A. Kogar, A. Zong, P. E. Dolgirev, X. Shen, J. Straquadine, Y.-Q. Bie, X. Wang, T. Rohwer, I.-C. Tung, Y. Yang, R. Li, J. Yang, S. Weathersby, S. Park, M. E. Kozina, E. J. Sie, H. Wen, P. Jarillo-Herrero, I. R. Fisher, X. Wang, N. Gedik, Light-induced charge density wave in $LaTe_3$. *Nat. Phys.* **16**, 159–163 (2020).
9. J. G. Horstmann, H. Böckmann, B. Wit, F. Kurtz, G. Storeck, C. Ropers, Coherent control of a surface structural phase transition. *Nature* **583**, 232–236 (2020).
10. R. T. Young, C. W. White, G. J. Clark, J. Narayan, W. H. Christie, M. Murakami, P. W. King, S. D. Kramer, Laser annealing of boron-implanted silicon. *Appl. Phys. Lett.* **32**, 139–141 (1978).
11. M. Combescot, J. Bok, Instability of the electron-hole plasma in silicon. *Phys. Rev. Lett.* **48**, 1413–1416 (1982).
12. H. W. Tom, G. D. Aumiller, C. H. Brito-Cruz, Time-resolved study of laser-induced disorder of Si surfaces. *Phys. Rev. Lett.* **60**, 1438–1441 (1988).
13. M. Harb, R. Ernstorfer, C. T. Hebeisen, G. Sciaini, W. Peng, T. Dartigalongue, M. A. Eriksson, M. G. Lagally, S. G. Kruglik, R. J. D. Miller, Electronically driven structure changes of Si captured by femtosecond electron diffraction. *Phys. Rev. Lett.* **100**, 155504 (2008).
14. P. Stampfli, K. H. Bennemann, Dynamical theory of the laser-induced lattice instability of silicon. *Phys. Rev. B Condens. Matter* **46**, 10686–10692 (1992).
15. P. Stampfli, K. H. Bennemann, Time dependence of the laser-induced femtosecond lattice instability of Si and GaAs: Role of longitudinal optical distortions. *Phys. Rev. B Condens. Matter* **49**, 7299–7305 (1994).
16. P. L. Silvestrelli, A. Alavi, M. Parrinello, D. Frenkel, Ab initio molecular dynamics simulation of laser melting of silicon. *Phys. Rev. Lett.* **77**, 3149–3152 (1996).
17. V. Recoules, J. Clerouin, G. Zerah, P. M. Anglade, S. Mazevet, Effect of intense laser irradiation on the lattice stability of semiconductors and metals. *Phys. Rev. Lett.* **96**, 055503 (2006).
18. E. S. Zijlstra, A. Kalitsov, T. Zier, M. E. Garcia, Squeezed thermal phonons precurse nonthermal melting of silicon as a function of fluence. *Phys. Rev. X* **3**, 011005 (2013).
19. N. Medvedev, Z. Li, B. Ziaja, Thermal and nonthermal melting of silicon under femtosecond x-ray irradiation. *Phys. Rev. B* **91**, 054113 (2015).
20. C. Lian, S. B. Zhang, S. Meng, Ab initio evidence for nonthermal characteristics in ultrafast laser melting. *Phys. Rev. B* **94**, 184310 (2016).
21. T. Pardini, J. Alameda, A. Aquila, S. Boutet, T. Decker, A. E. Gleason, S. Guillet, P. Hamilton, M. Hayes, R. Hill, J. Koglin, B. Kozioziemski, J. Robinson, K. Sokolowski-Tinten, R. Soufli, S. P. Hau-Riege, Delayed onset of nonthermal melting in single-crystal silicon pumped with hard x rays. *Phys. Rev. Lett.* **120**, 265701 (2018).
22. R. Darkins, P.-W. Ma, S. T. Murphy, D. M. Duffy, Simulating electronically driven structural changes in silicon with two-temperature molecular dynamics. *Phys. Rev. B* **98**, 024304 (2018).
23. N. Medvedev, M. Kopecky, J. Chalupsky, L. Juha, Femtosecond x-ray diffraction can discern nonthermal from thermal melting. *Phys. Rev. B* **99**, 100303(R) (2019).
24. P. Saeta, J. Wang, Y. Siegal, N. Bloembergen, E. Mazur, Ultrafast electronic disordering during femtosecond laser melting of GaAs. *Phys. Rev. Lett.* **67**, 1023–1026 (1991).
25. J. S. Graves, R. E. Allen, Response of GaAs to fast intense laser pulses. *Phys. Rev. B* **58**, 13627–13633 (1998).
26. K. J. Gaffney, A. M. Lindenberg, J. Larsson, K. Sokolowski-Tinten, C. Blome, O. Synnergren, J. Sheppard, C. Caleman, A. G. MacPhee, D. Weinstein, D. P. Lowney, T. Allison, T. Matthews, R. W. Falcone, A. L. Cavalieri, D. M. Fritz, S. H. Lee, P. H. Bucksbaum, D. A. Reis, J. Rudati, A. T. Macrander, P. H. Fuoss, C. C. Kao, D. P. Siddons, R. Pahl, K. Moffat, J. Als-Nielsen, S. Duesterer, R. Ischebeck, H. Schlarb, H. Schulte-Schrepping, J. Schneider, D. von der Linde, O. Hignette, F. Sette, H. N. Chapman, R. W. Lee, T. N. Hansen, J. S. Wark, M. Bergh, G. Huldt, D. van der Spoel, N. Timneanu, J. Hajdu, R. A. Akre, E. Bong, P. Krejcik, J. Arthur, S. Brennan, K. Luening, J. B. Hastings, Observation of structural anisotropy and the onset of liquidlike motion during the nonthermal melting of InSb. *Phys. Rev. Lett.* **95**, 125701 (2005).
27. A. M. Lindenberg, S. Engemann, K. J. Gaffney, K. Sokolowski-Tinten, J. Larsson, P. B. Hillyard, D. A. Reis, D. M. Fritz, J. Arthur, R. A. Akre, M. J. George, A. Deb,

P. H. Bucksbaum, J. Hajdu, D. A. Meyer, M. Nicoul, C. Blome, T. Tschentscher, A. L. Cavalieri, R. W. Falcone, S. H. Lee, R. Pahl, J. Rudati, P. H. Fuoss, A. J. Nelson, P. Krejcik, D. P. Siddons, P. Lorazo, J. B. Hastings, X-ray diffuse scattering measurements of nucleation dynamics at femtosecond resolution. *Phys. Rev. Lett.* **100**, 135502 (2008).
28. E. S. Zijlstra, J. Walkenhorst, M. E. Garcia, Anharmonic noninertial lattice dynamics during ultrafast nonthermal melting of InSb. *Phys. Rev. Lett.* **101**, 135701 (2008).
29. X. Wang, J. C. Ekström, Å. U. J. Bengtsson, A. Jarnac, A. Jurgilaitis, V. T. Pham, D. Kroon, H. Enquist, J. Larsson, Role of thermal equilibrium dynamics in atomic motion during nonthermal laser-induced melting. *Phys. Rev. Lett.* **124**, 105701 (2020).
30. C. W. Siders, A. Cavalleri, K. Sokolowski-Tinten, C. Tóth, T. Guo, M. Kammler, M. H. von Hoegen, K. R. Wilson, D. von der Linde, C. P. J. Barty, Detection of nonthermal melting by ultrafast X-ray diffraction. *Science* **286**, 1340–1342 (1999).
31. K. Sokolowski-Tinten, C. Blome, C. Dietrich, A. Tarasevitch, M. Horn von Hoegen, D. von der Linde, A. Cavalleri, J. Squier, M. Kammler, Femtosecond x-ray measurement of ultrafast melting and large acoustic transients. *Phys. Rev. Lett.* **87**, 225701 (2001).
32. J. A. Van Vechten, R. Tsu, F. W. Saris, D. Hoonhout, Reasons to believe pulsed laser annealing of Si does not involve simple thermal melting. *Phys. Lett. A* **74**, 417–421 (1979).
33. J. A. Van Vechten, R. Tsu, F. W. Saris, Nonthermal pulsed laser annealing of Si; plasma annealing. *Phys. Lett. A* **74**, 422–426 (1979).
34. C. V. Shank, R. Yen, C. Hirlimann, Time-resolved reflectivity measurements of femtosecond-optical-pulse-induced phase transitions in silicon. *Phys. Rev. Lett.* **50**, 454–457 (1983).
35. C. V. Shank, R. Yen, C. Hirlimann, Femtosecond-time-resolved surface structural dynamics of optically excited silicon. *Phys. Rev. Lett.* **51**, 900–902 (1983).
36. B. Rethfeld, K. Sokolowski-Tinten, D. von der Linde, S. I. Anisimov, Ultrafast thermal melting of laser-excited solids by homogeneous nucleation. *Phys. Rev. B* **65**, (2002).
37. M. Z. Mo, Z. Chen, R. K. Li, M. Dunning, B. B. L. Witte, J. K. Baldwin, L. B. Fletcher, J. B. Kim, A. Ng, R. Redmer, A. H. Reid, P. Shekhar, X. Z. Shen, M. Shen, K. Sokolowski-Tinten, Y. Y. Tsui, Y. Q. Wang, Q. Zheng, X. J. Wang, S. H. Glenzer, Heterogeneous to homogeneous melting transition visualized with ultrafast electron diffraction. *Science* **360**, 1451–1455 (2018).
38. S. R. Phillpot, S. Yip, D. Wolf, How do crystals melt? *Comput. Phys.* **3**, 20 (1989).
39. Z. Lin, L. V. Zhigilei, Time-resolved diffraction profiles and atomic dynamics in short-pulse laser-induced structural transformations: Molecular dynamics study. *Phys. Rev. B* **73**, (2006).
40. I. Inoue, Y. Deguchi, B. Ziaja, T. Osaka, M. M. Abdullah, Z. Jurek, N. Medvedev, V. Tkachenko, Y. Inubushi, H. Kasai, K. Tamasaku, T. Hara, E. Nishibori, M. Yabashi, Atomic-scale visualization of ultrafast bond breaking in x-ray-excited diamond. *Phys. Rev. Lett.* **126**, 117403 (2021).
41. P. Stampfli, K. H. Bennemann, Theory for the instability of the diamond structure of Si, Ge, and C induced by a dense electron-hole plasma. *Phys. Rev. B Condens. Matter* **42**, 7163–7173 (1990).
42. N. J. Hartley, J. Grenzer, L. Huang, Y. Inubushi, N. Kamimura, K. Katagiri, R. Kodama, A. Kon, W. Lu, M. Makita, T. Matsuoka, S. Nakajima, N. Ozaki, T. Pikuz, A. V. Rode, D. Sagae, A. K. Schuster, K. Tono, K. Voigt, J. Vorberger, T. Yabuuchi, E. E. McBride, D. Kraus, Using diffuse scattering to observe x-ray-driven nonthermal melting. *Phys. Rev. Lett.* **126**, 015703 (2021).
43. N. Medvedev, H. O. Jeschke, B. Ziaja, Nonthermal phase transitions in semiconductors induced by a femtosecond extreme ultraviolet laser pulse. *New J. Phys.* **15**, (2013).
44. T. Rohwer, S. Hellmann, M. Wiesenmayer, C. Sohrt, A. Stange, B. Slomski, A. Carr, Y. Liu, L. M. Avila, M. Kalläne, S. Mathias, L. Kipp, K. Rossnagel, M. Bauer, Collapse of long-range charge order tracked by time-resolved photoemission at high momenta. *Nature* **471**, 490–493 (2011).
45. C. W. Nicholson, A. Lücke, W. G. Schmidt, M. Puppin, L. Rettig, R. Ernstorfer, M. Wolf, Beyond the molecular movie: Dynamics of bands and bonds during a photoinduced phase transition. *Science* **362**, 821–825 (2018).
46. L. W. Wang, Natural orbital branching scheme for time-dependent density functional theory nonadiabatic simulations. *J. Phys. Chem. A* **124**, 9075–9087 (2020).
47. W.-H. Liu, Z. Wang, Z.-H. Chen, J.-W. Luo, S.-S. Li, L.-W. Wang, Algorithm advances and applications of time-dependent first-principles simulations for ultrafast dynamics. *WIREs Comput. Mol. Sci.* **12**, e1577 (2022).
48. K. Lu, Y. Li, Homogeneous nucleation catastrophe as a kinetic stability limit for superheated crystal. *Phys. Rev. Lett.* **80**, 4474–4477 (1998).
49. S. Mazevet, J. Clerouin, V. Recoules, P. M. Anglade, G. Zerah, Ab-initio simulations of the optical properties of warm dense gold. *Phys. Rev. Lett.* **95**, 085002 (2005).
50. Z. H. Jin, P. Gumbsch, K. Lu, E. Ma, Melting mechanisms at the limit of superheating. *Phys. Rev. Lett.* **87**, 055703 (2001).
51. W.-H. Liu, J.-W. Luo, S.-S. Li, L.-W. Wang, The critical role of hot carrier cooling in optically excited structural transitions. *npj Comput. Mater.* **7**, 117 (2021).
52. P. Yu, M. Cardona, *Fundamentals of Semiconductors* (Graduate Texts in Physics, Springer, 2010).
53. L. Waldecker, R. Bertoni, H. Hübener, T. Brumme, T. Vasileiadis, D. Zahn, A. Rubio, R. Ernstorfer, Momentum-resolved view of electron-phonon coupling in multilayer WSe_2. *Phys. Rev. Lett.* **119**, 036803 (2017).
54. S. Wall, S. Yang, L. Vidas, M. Chollet, J. M. Glownia, M. Kozina, T. Katayama, T. Henighan, M. Jiang, T. A. Miller, D. A. Reis, L. A. Boatner, O. Delaire, M. Trigo, Ultrafast disordering of vanadium dimers in photoexcited VO2. *Science* **362**, 572–576 (2018).
55. Z. Wang, S. S. Li, L. W. Wang, Efficient real-time time-dependent density functional theory method and its application to a collision of an ion with a 2D material. *Phys. Rev. Lett.* **114**, 063004 (2015).
56. D. R. Hamann, Optimized norm-conserving Vanderbilt pseudopotentials. *Phys. Rev. B* **88**, 085117 (2013).
57. W. Jia, Z. Cao, L. Wang, J. Fu, X. Chi, W. Gao, L.-W. Wang, The analysis of a plane wave pseudopotential density functional theory code on a GPU machine. *Comput. Phys. Commun.* **184**, 9–18 (2013).
58. W.-H. Liu, J.-W. Luo, S.-S. Li, L.-W. Wang, Impurity diffusion induced dynamic electron donors in semiconductors. *Phys. Rev. B* **100**, 165203 (2019).
59. L. Zhang, W. Chu, C. Zhao, Q. Zheng, O. V. Prezhdo, J. Zhao, Dynamics of photoexcited small polarons in transition-metal oxides. *J. Phys. Chem. Lett.* **12**, 2191–2198 (2021).
60. J. Ren, N. Vukmirović, L.-W. Wang, Nonadiabatic molecular dynamics simulation for carrier transport in a pentathiophene butyric acid monolayer. *Phys. Rev. B* **87**, 205117 (2013).
61. P. V. Parandekar, J. C. Tully, Detailed balance in Ehrenfest mixed quantum-classical dynamics. *J. Chem. Theor. Comput.* **2**, 229–235 (2006).
62. P. V. Parandekar, J. C. Tully, Mixed quantum-classical equilibrium. *J. Chem. Phys.* **122**, 094102 (2005).

Acknowledgments

Funding: The work in China was supported by the National Natural Science Foundation of China (NSFC) under grant nos. 11925407 and 61927901, the Key Research Program of Frontier Sciences, CAS under grant no. ZDBS-LY-JSC019, CAS Project for Young Scientists in Basic Research under grant no. YSBR-026, and the Strategic Priority Research Program of the Chinese Academy of Sciences under grant no. XDB43020000. L.-W.W. was supported by the Director, Office of Science, the Office of Basic Energy Sciences (BES), Materials Sciences and Engineering (MSE) Division of the U.S. Department of Energy (DOE) through the theory of material (KC2301) program under contract no. DEAC02-05CH11231. **Author contributions:** W.-H.L. performed the TDDFT simulations and prepared the figures. J.-W.L. and L.-W.W. proposed the research project, established the project direction, and conducted the analysis, discussion, and writing of the paper with input from W.-H.L. S.-S.L. provided the project infrastructure and supervised W.-H.L.'s study. **Competing interests:** The authors declare that they have no competing interests. **Data and materials availability:** All data needed to evaluate the conclusions in the paper are present in the paper and/or the Supplementary Materials. The rt-TDDFT code has been integrated into the PWmat package. The PWmat software can also be accessed directly from www.pwmat.com.

Submitted 27 November 2021
Accepted 23 May 2022
Published 6 July 2022
10.1126/sciadv.abn4430